

Better Source, Better Flow: Learning Condition-Dependent Source Distribution for Flow Matching

Junwan Kim^{1*} Jiho Park^{2*} Seonghu Jeon² Seungryong Kim^{2†}

¹New York University ² KAIST AI

<https://junwankimm.github.io/CSFM>

Abstract

Flow matching has recently emerged as a promising alternative to diffusion-based generative models, particularly for text-to-image generation. Despite its flexibility in allowing arbitrary source distributions, most existing approaches rely on a standard Gaussian distribution—a choice inherited from diffusion models—and rarely consider the source distribution itself as an optimization target in such settings. In this work, we show that *principled design of the source distribution is not only feasible but also beneficial* at the scale of modern text-to-image systems. Specifically, we propose learning a condition-dependent source distribution under the flow matching objective that better exploits rich conditioning signals. We identify key failure modes that arise when directly incorporating conditioning into the source, including distributional collapse and instability, and show that appropriate variance regularization and directional alignment between source and target are critical for stable and effective learning. We further analyze how the choice of target representation space impacts flow matching with structured sources, revealing regimes in which such designs are most effective. Extensive experiments across multiple text-to-image benchmarks demonstrate consistent and robust improvements, including up to a $3\times$ faster convergence in FID, highlighting the practical benefits of a principled source distribution design for conditional flow matching¹.

1. Introduction

Flow Matching (Lipman et al., 2022; Liu et al., 2022) has recently emerged as a powerful framework for generative modeling, demonstrating strong performance across many domains. In particular, Text-to-Image (T2I) systems show that *conditional* flow matching¹ can generate high-fidelity

*Equal contribution. †Corresponding author.

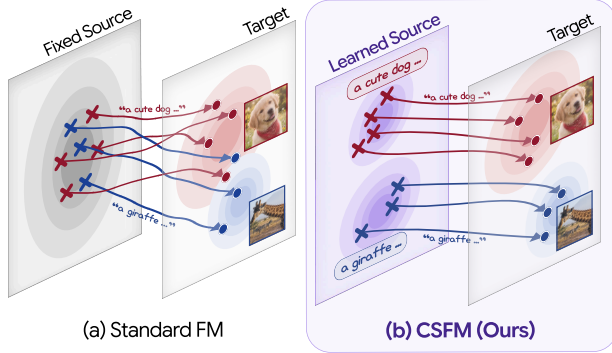


Figure 1. Condition-dependent Source Flow Matching (CSFM). Flow matching does not require the source distribution to be a fixed standard Gaussian. We leverage this flexibility by learning a condition-dependent source distribution, which reduces intrinsic variance and improves conditional flow matching performance.

images with strong prompt adherence (Esser et al., 2024; Labs, 2024), suggesting that it is a promising alternative to diffusion-based models for conditional image generation.

At its core, flow matching learns a continuous-time velocity field that transports samples from a *source* distribution to a target distribution. Unlike diffusion models, which rely on stochastic noise injection (Ho et al., 2020; Song et al., 2020a), or denoising score matching (Song et al., 2020b; Song & Ermon, 2019), flow matching directly models deterministic dynamics. More importantly, it imposes no restriction on the choice of the source distribution. In principle, this flexibility makes flow matching particularly appealing for conditional generation with rich conditioning signals.

Despite this conceptual advantage, most existing flow matching methods still adopt a standard Gaussian—which carries no information about the data distribution—as the source distribution. This design choice is largely inherited from diffusion models and motivated by simplicity rather than by the structure of the conditional generation problem itself. Some recent works (Issachar et al., 2025; Lee et al., 2025)

¹In this paper, *conditional* flow matching refers to flow matching conditioned on an external variable. This should not be confused with Conditional Flow Matching (CFM) (Lipman et al., 2022), where “conditional” instead refers to conditioning on X_1 .

have questioned whether standard Gaussian noise is an appropriate starting point for transporting mass toward highly structured and multimodal data distributions. Prior efforts in this direction typically pursue either improved couplings within a Gaussian source—often via optimal transport—or alternative source distributions learned from data.

However, extending these approaches to conditional settings such as text-to-image generation introduces additional challenges. Optimal transport-based methods typically require solving matching problems within each minibatch (Cheng & Schwing, 2025; Tong et al., 2023a). This batch-level optimization becomes a significant computational bottleneck in text-to-image models, where training involves large-scale datasets and high-dimensional signals. Other lines of work investigate source-guided or learned source distributions and report promising results, but these methods are largely limited to unconditional or discrete class-conditional settings (Issachar et al., 2025; Lee et al., 2025). As a result, their applicability to text-to-image generation with complex conditioning signals remains unclear.

Recent works such as CrossFlow and FlowTok (Liu et al., 2025; He et al., 2025) move closer to this regime by learning flow matching directly between text and image distributions. These methods demonstrate that incorporating conditioning information into the source distribution is feasible within flow matching models, even at the scale required for text-to-image generation. Nevertheless, the empirical gains reported so far are relatively limited, suggesting that fully realizing the benefits of incorporating conditioning information into the source distribution requires more careful design.

To this end, we propose *Condition-dependent Source Flow Matching* (CSFM), demonstrating that source distribution design is not only feasible but also beneficial in practical text-to-image settings, facilitating more efficient and effective training of complex conditional generative models. Specifically, (1) we show that stable and effective learning with condition-dependent sources requires careful regularization and alignment: we identify key failure modes such as collapse and optimization challenges, and demonstrate that appropriate variance regularization together with source–data directional alignment is crucial for stabilization; (2) we show that the effectiveness of learning source distributions depends on the choice of target representation space, and identify representation regimes in which flow matching benefits most from source design; and (3) through extensive experiments and ablation studies across multiple text-to-image benchmarks, we demonstrate consistent and robust empirical improvements, including up to a **3.01**× faster convergence in FID, and **2.48**× faster convergence in CLIP Score, providing strong evidence that principled source design enables flow matching to better exploit conditioning information in practice.

2. Preliminaries

2.1. Flow Matching

Flow Matching (FM) defines a generative process by solving an ordinary differential equation (ODE):

$$\frac{d}{dt} X_t = v_\theta(X_t, t), \quad t \in [0, 1], \quad (1)$$

where $v_\theta(\cdot, t)$ is a neural vector field parameterized by θ . The goal of FM is to find θ such that the push-forward of a source distribution p_0 through the ODE matches a target data distribution p_1 .

Typically, we consider a probability path p_t and an associated marginal velocity field u_t that generates p_t . For a given coupling $(X_0, X_1) \sim \pi(x_0, x_1)$ where $X_0 \sim p_0$ and $X_1 \sim p_1$, we define the conditional velocity as:

$$\Delta := X_1 - X_0. \quad (2)$$

Assuming a linear interpolation path $X_t = (1 - t)X_0 + tX_1$, the marginal velocity field at a point x and time t is expressed as the conditional expectation:

$$u_t(x) = \mathbb{E}[\Delta \mid X_t = x]. \quad (3)$$

The Flow Matching objective minimizes the mean squared error between the neural vector field and the conditional velocity:

$$\mathcal{L}_{\text{FM}}(\theta) = \mathbb{E}_{t, \pi(X_0, X_1)} [\|v_\theta(X_t, t) - \Delta\|^2], \quad (4)$$

where $t \sim p(t)$ is a probability distribution over $[0, 1]$. While each conditional path $t \mapsto X_t$ is linear, the learned marginal vector field v_θ generally induces curved trajectories because it aggregates multiple, potentially conflicting velocities Δ at each spacetime point (x, t) .

For conditional flow matching, target X_1 is naturally paired with a conditioning variable C , resulting in:

$$\mathcal{L}_{\text{FM}}(\theta) = \mathbb{E}_{t, \pi(X_0, X_1, C)} [\|v_\theta(X_t, t, C) - \Delta\|^2]. \quad (5)$$

2.2. Decomposition of Flow Matching Loss

To analyze the learning dynamics, the FM objective in Eq. (4) can be decomposed (See Appx. C) into two components:

$$\begin{aligned} \mathcal{L}_{\text{FM}}(\theta) &= \underbrace{\mathbb{E}_{t, \pi(X_0, X_1)} [\|v_\theta(X_t, t) - u_t(X_t)\|^2]}_{\text{Approximation Error}} \\ &+ \underbrace{\mathbb{E}_{t, \pi(X_0, X_1)} [\text{Var}(\Delta \mid X_t)]}_{\text{Intrinsic Variance}}. \end{aligned} \quad (6)$$

The Approximation Error represents the model’s ability to recover the marginal velocity field u_t . The Intrinsic Variance

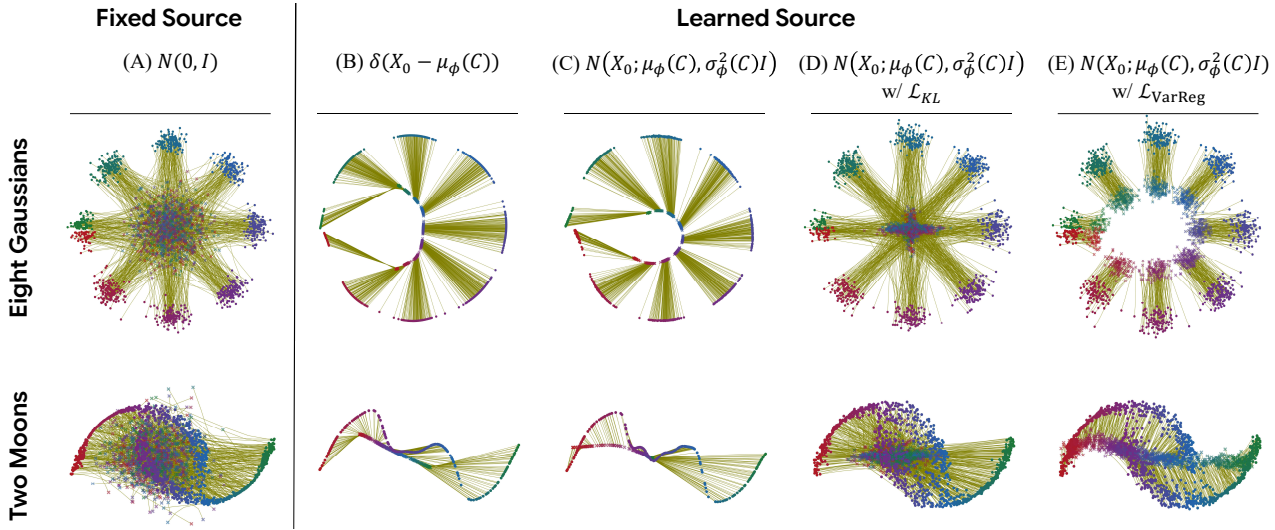


Figure 2. Analysis of CSFM designs. We investigate the effect of the source designs using two two-dimensional synthetic datasets with continuous conditions: Eight Gaussians with polar angle condition and Two Moons with x -coordinate condition. We visualize the transport trajectories, where ‘ \times ’ denotes source points X_0 and ‘ \bullet ’ denotes points X_1^{sampled} generated by the flow model. Colors indicate the conditioning variable. **(A) Fixed Standard Gaussian:** Independent coupling results in entangled paths and high intrinsic variance. **(B) Deterministic Mapping:** The flow model with a deterministically mapped source fails to reconstruct the original target distribution. **(C) Conditional Gaussian:** Although the source is modeled as a condition-dependent Gaussian, its variance collapses during training, resulting in insufficient support and an inability to recover the target distribution. **(D) Conditional Gaussian with Standard KL regularization:** While preventing collapse to a deterministic mapping, the constraint on $\mu_\phi(C)$ limits the mobility of the source, yielding entangled trajectories. **(E) Conditional Gaussian with Variance Regularization:** Variance Regularization prevents collapse while allowing the conditional mode $\mu_\phi(C)$ to move, resulting target-aligned source distribution and disentangled trajectories.

is the irreducible error determined by the choice of coupling π . A high intrinsic variance implies that the mapping from X_t to Δ is multi-valued; that is, multiple trajectories originating from different X_0 or X_1 intersect at the same (x, t) , providing inconsistent supervision signals to the model.

Prior works on optimal transport couplings (Tong et al., 2023a; Pooladian et al., 2023) show that reducing intrinsic variance in Eq. (6) (Tong et al., 2023a) leads to faster convergence and more stable flow learning. More precisely, these works propose replacing the independent coupling $\pi(X_0, X_1) = p_0(X_0)p_1(X_1)$ with an optimal transport coupling that explicitly minimizes path intersections, resulting in less entangled and smoother transport trajectories (Ma et al., 2025). Through improved coupling, this approach yields cleaner supervision signals with lower gradient variance (Pooladian et al., 2023), facilitating more accurate velocity estimation and enhanced sample quality. However, these methods are less practical in high-dimensions, where the approximation error increases with dimensionality.

3. Method

In this section, we present *Condition-dependent Source Flow Matching* (CSFM), a framework that transforms a fixed source distribution into a learnable, condition-dependent distribution for flow matching (Fig. 1). This formulation enables adaptive coupling design that reduces transport path

complexity. We detail the construction of the learnable coupling, and introduce targeted regularization strategies to prevent source collapse and maintain sufficient support, together with alignment objectives that improve training dynamics under complex conditioning.

3.1. Learnable Conditional Source Distribution

In conditional generation scenarios such as text-to-image generation, the conditioning variable C is naturally paired with the data random variable X_1 . We leverage this relationship to design a flexible source distribution by introducing a learnable, condition-dependent source distribution $p_\phi(X_0|C)$. This defines a learnable coupling $\pi_\phi(X_0, X_1, C) = p_\phi(X_0|C)p_1(X_1, C)$ with parameters ϕ .

Specifically, we introduce a source generator $g_\phi(\cdot)$ that maps the conditioning variable C into the source space, such that $X_0 = g_\phi(C)$. We then jointly train the flow model $v_\theta(\cdot)$ and the source generator g_ϕ under the conditional FM loss:

$$\mathcal{L}_{\text{FM}}(\theta, \phi) = \mathbb{E}_{t, \pi_\phi(X_0, X_1, C)} \left[\|v_\theta(X_t, t, C) - \Delta\|^2 \right] \quad (7)$$

where $\Delta = X_1 - g_\phi(C)$,

$$X_t = (1-t)g_\phi(C) + tX_1.$$

This formulation enables end-to-end learning of the source-target coupling, effectively transforming the previously ir-

reducible intrinsic variance term (Eq. (6)) into a learnable component through adaptive coupling design.

3.2. Designing Conditional Source Distribution

While a learnable conditional source distribution allows for variance reduction, careful design is required to ensure that the induced flow fields recover the target distribution.

Conditional Gaussian for sufficient support. A straightforward design for source would be a deterministic mapping, $p_\phi(X_0|C) = \delta(X_0 - \mu_\phi(C))$ (i.e., $x_0 = g_\phi(c)$). However, this choice severely restricts the support² of the source X_0 . As established by Lee et al. (2025), an overly concentrated source (i.e., insufficient source support) causes path entanglement and degrades flow matching performance. We empirically demonstrate this failure mode for deterministic conditional sources in toy experiments (Fig. 2 (B)), where the flow model fails to recover the distribution of X_1 . To address this problem, we model the generator as a conditional Gaussian distribution:

$$g_\phi(C) \sim \mathcal{N}(\mu_\phi(C), \sigma_\phi^2(C)\mathbf{I}), \quad (8)$$

which theoretically ensures full support for $\sigma_\phi^2 > 0$, with smooth and continuous embedding.

Variance regularization for collapse prevention. Despite the Gaussian parameterization, joint training with the flow model often drives the conditional variance $\sigma_\phi^2(C) = \text{Var}(X_0|C)$ toward zero (Fig. 2 (C)), since shrinking the source variance directly reduces the intrinsic variance term in Eq. (6). To counteract this effect, a common strategy when parameterizing conditional Gaussians is to regularize the distribution toward a standard normal prior (Liu et al., 2025; He et al., 2025). However, such regularization implicitly constrains both the variance and the mean, forcing $\mu_\phi(C)$ toward the origin, which we find unnecessarily restricts the flexibility of the source distribution and degrades performance. As illustrated in Fig. 2 (D), this constraint prevents the source from relocating toward target modes, resulting in entangled transport paths that offer little improvement over a fixed Gaussian source (Fig. 2 (A)). To avoid this limitation, we adopt a variance-only regularization that penalizes deviations of $\sigma_\phi^2(C)$ from a unit variance while leaving the mean $\mu_\phi(C)$ unconstrained:

$$\mathcal{L}_{\text{VarReg}}(\phi) = \mathbb{E}_C \left[D_{\text{KL}} \left(\mathcal{N}(\mu_\phi(C), \sigma_\phi^2(C)\mathbf{I}) \parallel \mathcal{N}(\mu_\phi(C), \mathbf{I}) \right) \right] \quad (9)$$

By allowing $\mu_\phi(C)$ to move freely, the source distribution autonomously shifts toward the target modes while main-

taining sufficient support (Fig. 2 (E)). This relocation significantly reduces path intersections and simplifies the velocity field complexity, providing cleaner supervision signals.

3.3. Direct Source-Target Alignment for Complex Conditional Distribution

Unlike simplified toy settings, practical conditional generation tasks such as text-to-image synthesis involve highly complex and multimodal relationships between the condition C and the target data X_1 . Modern text-to-image architectures (Esser et al., 2024; Labs, 2024; Qin et al., 2025) are specifically designed to model such complexity by tightly integrating the conditioning signal into the flow model $v_\theta(\cdot)$, allowing the conditional information to directly modulate the vector field itself. However, this tight integration also makes the optimization of a suitable source distribution more challenging. Since the flow model can account for most of the conditional information through C , minimizing the flow matching objective imposes weaker supervision signals for the source distribution, making it harder to learn an informative source in practice (see Appx. B for a detailed analysis).

To fully leverage modern conditional architectures while mitigating this optimization challenge, we introduce an explicit source–target alignment objective. Motivated by recent findings that directional information is critical in high-dimensional flow matching (Lee et al., 2025), we adopt a negative cosine similarity loss to encourage directional alignment between the learned source and target samples:

$$\mathcal{L}_{\text{align}}(\phi) = \mathbb{E}_{C, X_1} \left[1 - \frac{X_0 \cdot X_1}{\|X_0\| \|X_1\|} \right]. \quad (10)$$

Combined with the flow matching loss \mathcal{L}_{FM} and the variance regularization $\mathcal{L}_{\text{VarReg}}$, the final training objective is:

$$\mathcal{L}_{\text{total}} = \mathcal{L}_{\text{FM}} + \lambda_{\text{VarReg}} \mathcal{L}_{\text{VarReg}} + \lambda_{\text{align}} \mathcal{L}_{\text{align}}, \quad (11)$$

where λ_{VarReg} and λ_{align} are hyperparameters that balance the distribution support and alignment quality of the learned source distribution, respectively.

4. Experiments

In this section, we first validate the key components analyzed in our toy experiments within a practical text-to-image generation framework. We then demonstrate that CSFM improves generation performance, accelerates training convergence, yields straighter flows, and scales effectively. Finally, we analyze the impact of the target representation on CSFM.

Implementation Details. We use RAE (DINOv2) (Zheng et al., 2025) as the default target image representation and adopt a DDT head (Wang et al., 2025a) to provide sufficient

²The support of a random variable X is defined as the smallest closed set $S \subseteq \mathbb{R}^d$ such that $\mathbb{P}(X \in S) = 1$.

Table 1. Component-wise analysis on ImageNet 256×256. We analyze the effect of individual components on the captioned ImageNet-1K dataset. All models are trained for 100K iterations with a batch size of 1024 and evaluated using a 50-step Euler ODE sampler without guidance. Baseline models with a fixed Gaussian source are highlighted in gray, **bold** entries denote the default setting for subsequent experiments, and underlined values indicate the best results. In this experiment, RAE (DINOv2) is used as the image autoencoder. [†] denotes a baseline model with increased parameters to approximately match the parameter count introduced by the source generator.

Source Distribution	Text Encoder	Flow Backbone	Align Loss	Reg. Loss	FID ↓	CLIP ↑	IS↑	sFID↓	Prec.↑	Recall↑
$\mathcal{N}(0, I)$	CLIP	LightningDiT			3.721	0.3283	169.2	6.175	0.7977	0.5718
		MMDiT	X	X	3.412	0.3399	186.1	6.507	0.7906	0.5747
		UnifiedNextDiT			3.036	0.3398	187.0	5.859	0.7917	0.5881
		UnifiedNextDiT [†]			2.925	0.3396	189.1	5.730	0.7898	0.5974
$p_\phi(X_0 C)$	CLIP	UnifiedNextDiT	X	KL	NaN	NaN	NaN	NaN	NaN	NaN
			X	VarReg	2.904	<u>0.3405</u>	190.1	5.671	0.7869	0.5913
			MSE	VarReg	2.765	0.3404	<u>195.6</u>	<u>5.630</u>	0.7921	<u>0.5958</u>
	CLIP	UnifiedNextDiT	X	CosSim	2.765	0.3404	195.6	5.630	0.7921	0.5958
	CLIP	LightningDiT MMDiT UnifiedNextDiT	CosSim	VarReg	2.942	0.3410	195.5	6.247	0.7896	0.5902
	CLIP				2.453	0.3420	203.7	5.491	0.7947	0.6029
	CLIP				3.041	0.3363	191.9	5.972	0.7961	0.5791
Qwen-3	CLIP	UnifiedNextDiT	CosSim	VarReg	3.051	0.3415	199.0	6.339	<u>0.7978</u>	0.5745
					2.453	0.3420	203.7	<u>5.491</u>	0.7947	<u>0.6029</u>
	CLIP	UnifiedNextDiT	CosSim	VarReg	2.453	<u>0.3420</u>	203.7	5.491	0.7947	<u>0.6029</u>
	Qwen-3				2.519	0.3409	200.5	<u>5.465</u>	0.7953	0.6009

model capacity for the high-dimensional feature space. The motivation for the target representation choice, along with a deeper analysis, is discussed in Sec. 4.3. To facilitate fair evaluation at an appropriate scale for practical text-to-image generation tasks, we construct a benchmark dataset based on ImageNet-1K (Russakovsky et al., 2015). We employ Qwen3-VL (Bai et al., 2025a) to generate descriptive captions for images (see Fig. 12), rather than simple class-level captions. Model performance is primarily evaluated using FID (Heusel et al., 2017) and CLIP Score (Hessel et al., 2021), together with Inception Score (IS) (Salimans et al., 2016), sFID, and Precision–Recall metrics on the validation set. For ImageNet-1K evaluation, images are generated from validation captions. Unless otherwise specified, all evaluations are conducted without any guidance. Additional training and evaluation details are provided in Appx. D.

4.1. Component-wise Analysis

Choice of source regularization matters. We examine the role of the regularization loss $\mathcal{L}_{\text{VarReg}}$ in stabilizing source learning. Using CLIP (Radford et al., 2021) as the text encoder, we evaluate how variance regularization affects model behavior. Without any regularization, the learned source distribution collapses, driving the training objective near zero and preventing meaningful generation. Standard KL regularization avoids this collapse and improves upon a fixed Gaussian source, but the gains remain limited. As discussed in Sec. 3.2, this is due to the KL regularization constraining the source mean $\mu_\phi(C)$ toward the origin, which restricts source mobility. In contrast, our variance regularization preserves variance control while allowing the mean

to adapt freely, enabling effective alignment with the target distribution. This design already yields clear improvements across all evaluation metrics, highlighting the importance of unconstrained mean adaptation for learning expressive source distributions in large-scale text-to-image generation.

Alignment is effective in complex settings. We next examine the role of the alignment loss $\mathcal{L}_{\text{align}}$ in improving optimization when learning condition-dependent sources under complex conditioning. As discussed in Sec. 3.3, strong conditioning in the flow model $v_\theta(\cdot)$ can substantially weaken the learning signal available to the source, making optimization unstable and often resulting in a poorly trained source distribution (see Appx. B). In this setting, we observe that directional alignment provides substantial improvements and effectively mitigates these optimization difficulties. Importantly, CSFM without the alignment loss exhibits higher FM loss with increased gradient variance in Fig. 3. This indicates that the alignment objective improves flow matching optimization itself rather than serving as an external regularizer. A more detailed discussion of these statistics is provided in Sec. 4.2. To further highlight the importance of directional alignment, we compare this approach with an MSE-based alignment objective and find that minimizing the ℓ_2 distance between X_0 and X_1 overly restricts the source distribution, limiting its flexibility under the FM objective and leading to degraded performance.

Robustness to conditioning architecture. We evaluate whether CSFM is consistently effective across different conditioning architectures. We consider three representative paradigms in modern text-to-image generation: Light-

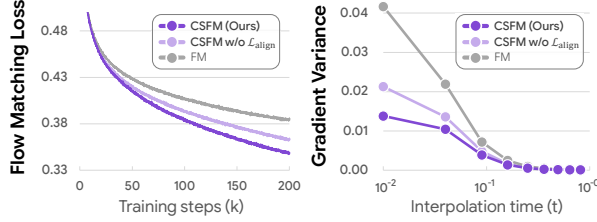


Figure 3. Flow matching loss and gradient variance. ($\text{Var}(\nabla_\theta \mathcal{L}_{\text{FM}})$). We compare the training dynamics of standard FM, CSFM without alignment loss, and CSFM. CSFM achieves faster loss convergence and lower gradient variance, particularly at early interpolation times near the source. Details of the measurement are provided in Appx. F.

ningDiT (Yao et al., 2025), which injects conditioning primarily via adaptive layer normalization (AdaLN) (Peebles & Xie, 2023); MMDiT (Esser et al., 2024), which adopts a dual-stream design that processes text and image tokens in separate but interacting branches; and UnifiedNextDiT (Qin et al., 2025), which employs a unified sequence representation with Multimodal RoPE (mRoPE) (Bai et al., 2025b) to capture cross-modal structure without explicit modulation layers. As shown in Tab. 1, our method consistently improves performance over the baseline across all three architectures. These results indicate that CSFM yields robust gains in text-to-image generation, independent of the specific conditioning mechanism used by the backbone.

Robustness to text encoders. We further assess the robustness of our method by replacing the CLIP text encoder with a large language model (LLM). Specifically, we use Qwen3-0.6B (Yang et al., 2025) as the text encoder and observe that our method maintains comparable performance to the CLIP-based setting. This result indicates that our framework generalizes across different text encoder architectures and is not tied to a specific encoder design.

Unless otherwise specified, all subsequent experiments adopt the default configuration highlighted in **bold** in Tab. 1.

4.2. Advantages of CSFM

CSFM improves training dynamics of flow matching. Modeling a condition-dependent source enables the reduction of the intrinsic variance term in Eq. (6), leading to markedly improved optimization dynamics for flow matching. As shown in Fig. 3, CSFM achieves a faster decrease in the FM loss, indicating accelerated convergence (Benton et al., 2023a;b). Looking more closely at the optimization behavior, effective source–target coupling is known to reduce the gradient variance of the FM loss (Pooladian et al., 2023). We empirically examine this behavior by measuring the gradient variance at 100K training steps in Fig. 3. CSFM consistently attains lower gradient variance than the baseline, with pronounced gains at small interpolation times (i.e., near the source). This suggests that the condition-dependent

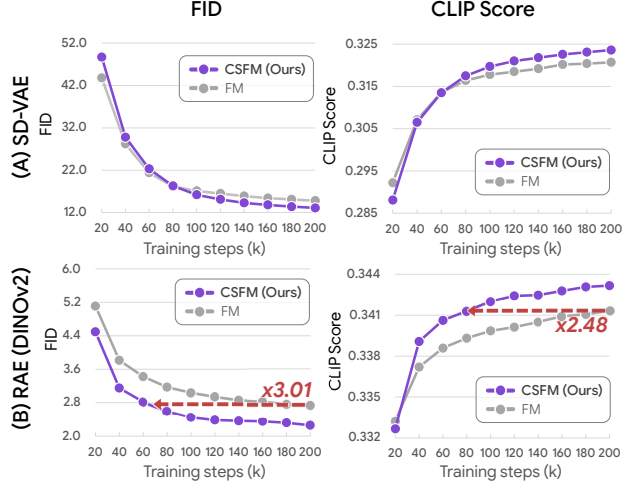


Figure 4. Training efficiency under different target representations. We compare FID and CLIP score trajectories between CSFM and FM, using (A) SD-VAE and (B) RAE (DINOv2) target representations on the ImageNet-1K validation set. While CSFM yields consistent gains under both representations, it substantially accelerates convergence and achieves larger improvements in the structured RAE space.

source practically reduces the intrinsic variance of FM loss and provides cleaner supervision signals.

CSFM improves flow matching performance. We show that the improved training dynamics translate into performance gains. As shown in Fig. 4, CSFM achieves consistent improvement, yielding a $3.01 \times$ speedup in FID convergence and a $2.48 \times$ speedup in CLIP score in the RAE (Zheng et al., 2025) latent space. We take a deeper look at the performance discrepancy between SD-VAE and RAE in Sec. 4.3. Qualitatively, CSFM tends to better reflect complex text conditioning involving multiple objects and relationships, while preserving high visual fidelity, as illustrated in Fig. 15.

CSFM straightens transport paths. Reducing the intrinsic variance in Eq. (6) is known to minimize path intersections and induces straighter flow fields (Tong et al., 2023a; Ma et al., 2025). We therefore evaluate flow straightness via few-step generation. As shown in Fig. 5 (A), CSFM degrades more gracefully than standard FM as the number of sampling steps decreases: when reducing from 50 to 3 steps, FID degrades by 8.75 for CSFM compared to 12.47 for the baseline. To further investigate the potential straightness of the learned source distribution, we conduct 1-Reflow (Liu et al., 2022) experiments. Reflow rectifies the flow fields and improves few-step generation, by fine-tuning the flow model on sampled pairs ($X_0, X_1^{\text{sampled}}$). We fine-tune the flow models for 20K steps from 100K-steps checkpoint, while freezing the source generator for CSFM. As shown in Fig. 5 (B), CSFM exhibits substantially straighter flow fields: reducing from 50 to 2 sampling steps, FID degrades by only 3.51, whereas standard FM suffers a larger degrada-

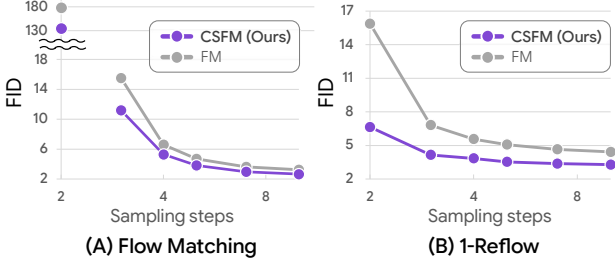


Figure 5. Few-step generation and flow straightness. We compare FID across different sampling steps for (A) Flow Matching and (B) 1-Reflow. CSFM degrades more gracefully as the number of steps decreases, indicating reduced path intersections and a straighter transport field compared to the FM baseline.

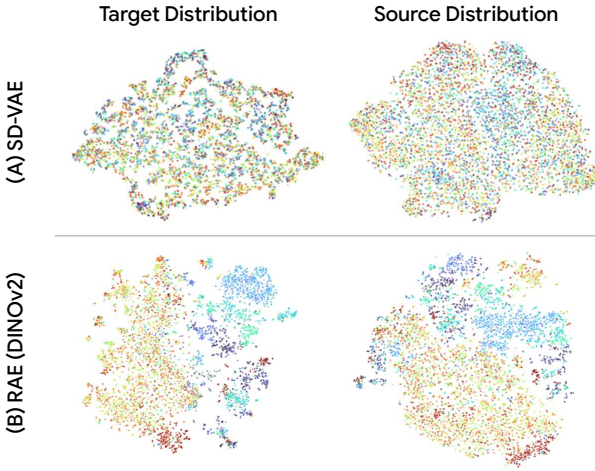


Figure 6. t-SNE visualization of target and learned source distributions. We visualize t-SNE embeddings of target (left) and corresponding learned source (right) distributions, colored by class labels, for (A) SD-VAE and (B) RAE (DINOv2) representations. The entangled SD-VAE space leads to an equally entangled learned source, whereas the structured RAE space enables a semantically organized source distribution.

tion of 11.75. These results provide empirical evidence that the learned source distribution reduces path intersections and induces straighter flow fields.

CSFM outperforms existing condition-aware coupling methods. We compare CSFM with existing flow matching approaches that modify source-target coupling based on the condition (Tab. 2). C^2OT (Cheng & Schwing, 2025) employs condition-aware optimal transport couplings to improve training paths; however, in high-dimensional settings it suffers from approximation errors and limited scalability, leading to degraded performance relative to standard FM. CrossFlow (Liu et al., 2025) introduces a text-dependent source generator, but its design primarily targets cross-modal transport rather than improving flow matching, resulting in no improvement over the baseline. In contrast, CSFM adopts a principled coupling that explicitly targets the reduction of intrinsic variance in Eq. (6), yielding consistent

Table 2. Comparison between condition aware coupling methods on ImageNet 256×256. We compare methods that learn a text-dependent source distribution (CrossFlow) or perform text-aware coupling among Gaussian source distribution (C^2OT). All baselines are reproduced adopting RAE (DINOv2) for target latent and using identical model architectures for fair comparison.

Method	FID ↓	CLIP ↑
Standard FM	2.925	0.3396
CrossFlow (Liu et al., 2025)	2.957	0.3301
C^2OT (Cheng & Schwing, 2025)	3.365	0.3406
CSFM (Ours)	2.453	0.3433

Table 3. Guidance analysis on ImageNet 256×256. We investigate the effect of guidance using AutoGuidance (AG) (Karras et al., 2024), comparing our method and flow matching with a fixed Gaussian source, both exhibiting comparable gains from guidance.

Method	FID ↓	CLIP ↑
Standard FM	3.036	0.3398
Standard FM + AG	2.673	0.3400
CSFM (Ours)	2.453	0.3420
CSFM (Ours) + AG	2.016	0.3433

and significant improvements over both existing methods and the baseline.

CSFM remains effective with guidance. Because the learned source X_0 already encodes conditional information, our framework does not naturally admit a truly unconditional variant; consequently, we do not adopt classifier-free guidance (CFG) (Ho & Salimans, 2022). Instead, following prior observations that autoguidance (Karras et al., 2024) is more appropriate than CFG in the RAE feature space (Zheng et al., 2025), we evaluate our method with autoguidance. As shown in Tab. 3, CSFM achieves performance gains comparable to those observed in the no-guidance setting.

4.3. Target Representation Matters

In Fig. 4, CSFM improves performance across image representation spaces, but with much larger gains in RAE (DINOv2) (Zheng et al., 2025) latents than in SD-VAE (Dhariwal & Nichol, 2021). This indicates that the structure of the target representation is critical for effective source learning.

At a high level, learning a condition-dependent source is most beneficial when the conditioning signal C induces a well-separated and discriminative structure in the target space, as illustrated in Fig. 2. In such cases, samples associated with the same condition form relatively compact clusters, allowing the source mean $\mu_\phi(C)$ to be well-defined and aligned with the target distribution. This reduces path intersections and lowers the intrinsic variance in Eq. (6), leading to more coherent supervision for flow matching.

However, this advantage diminishes when a single condi-



Figure 7. **Qualitative samples** generated by CSFM (1.3B). Images are generated at 224×224 resolution using DPG-Bench prompts.

tioning signal corresponds to a highly multimodal target distribution. As demonstrated in Appx. A.3, when samples associated with the same C are spread across distant modes, the source mean becomes ambiguous. This ambiguity leads to frequent path intersections, conflicting supervision signals, and persistently high intrinsic variance. In such extreme cases, the learned source exhibits behavior similar to a fixed Gaussian prior, providing limited additional benefit.

This property makes CSFM most effective when paired with representation autoencoders that operate in structured latent spaces, such as DINOv2 (Oquab et al., 2023) or SigLIP2 (Tschannen et al., 2025). In these spaces, samples associated with the same conditioning signal tend to be more concentrated (Huh et al., 2024; Wybitul et al., 2026; Bolya et al., 2025), reducing multimodality with respect to C . This concentration simplifies source learning and allows CSFM to be applied more effectively.

We further support this analysis with t-SNE visualizations in Fig. 6, where points are color-coded by their corresponding classes. In the SD-VAE representation, the target distribution exhibits strong entanglement and weak structure with respect to the conditioning signal, and this lack of structure is reflected in a similarly non-discriminative learned source (Fig. 6 (A)). In contrast, the RAE (DINOv2) representation induces a more organized target geometry, which in turn allows the source distribution to become more discriminative and results in larger performance gains (Fig. 6 (B)).

4.4. Scaling CSFM

To examine whether CSFM remains effective at scale, we scale our default configuration from Tab. 1 to a 1.3B-parameter model, replacing the text encoder with Qwen3-0.6B to better handle longer text inputs. The model is first pretrained on the BLIP3o pretraining dataset (Chen et al., 2025b), which contains approximately 36M samples, and

Table 4. **Large-scale text-to-image evaluation.** Results on GenEval and DPG-Bench. We report standard FM and CSFM with UnifiedNextDiT (1.3B), together with results from prior work that evaluate the same model families at different parameter scales, to contextualize the magnitude of performance gains at this scale.

Model	#Params	GenEval	DPG-Bench
BLIP3o (Chen et al., 2025b)	4B	0.81	79.36
	8B	0.84	81.60
Sana (Xie et al., 2024)	0.6B	0.64	83.60
	1.6B	0.66	84.80
Standard FM	1.3B	0.77	78.31
CSFM (Ours)	1.3B	0.80	81.11

then finetuned on BLIP3o-60K dataset. We adopt a SigLIP2-based RAE decoder (Tong et al., 2026) which operates on 224×224 resolution, and evaluate the resulting model on GenEval (Ghosh et al., 2023) and DPG-Bench (Hu et al., 2024). As shown in Tab. 4, even at this scale, the proposed approach consistently outperforms the Gaussian-source baseline across all benchmarks, demonstrating that learnable source distributions remain effective for high-capacity text-to-image generation. We visualize samples from the 1.3B model in Fig. 7, with full results in Appx. H.

However, as standard text-to-image benchmarks become increasingly saturated at this scale, quantitative metrics alone provide a limited view of model behavior. We therefore additionally present qualitative comparisons in Fig. 16 and Fig. 17, which better illustrate the perceptual differences induced by source design and provide complementary evidence of the benefits of our approach in large-scale settings.

5. Related Works

We discuss the most relevant related work here and provide additional details in Appx. G.

Recent studies have explored incorporating conditioning information into the source distribution for flow matching, including learning condition-dependent sources via regression objectives (Issachar et al., 2025), diffusion-based inversion (Ahn et al., 2024), geometric and optimization-driven source design (Lee et al., 2025), or reparameterization schemes that prevent collapse (Chen et al., 2025a). Other lines of work extend flow matching to transport between different modalities, such as text and images, often using auxiliary encoders or contrastive objectives (Liu et al., 2025; He et al., 2025). While these approaches demonstrate the feasibility of learning structured sources or cross-modal couplings, they typically rely on multi-stage pipelines, remain small-scale or simple conditional settings, or show limited gains in complex generative scenarios. In contrast, our work studies how principled, condition-dependent source design can improve flow matching dynamics and generative performance in large-scale text-to-image models.

6. Conclusion

In this work, we present *Condition-dependent Source Flow Matching* (CSFM), demonstrating that principled design of the source distribution can improve flow matching models by facilitating more favorable training dynamics and leading to consistent performance gains. Through extensive experiments and analyses, we elucidate the core mechanisms underlying our approach and show how condition-dependent source design enables more efficient and stable learning in complex conditional generation settings.

Impact Statement

This paper presents work whose goal is to advance the field of Machine Learning, specifically in the area of generative modeling. While generative models have many potential societal consequences, these are largely well understood in the existing literature. As with other generative image models, the proposed method may generate harmful or inappropriate content depending on the training data and prompts, highlighting the importance of responsible dataset curation and deployment. We do not identify additional societal impacts that require specific discussion beyond these established considerations.

References

Ahn, D., Kang, J., Lee, S., Min, J., Kim, M., Jang, W., Cho, H., Paul, S., Kim, S., Cha, E., Jin, K. H., and Kim, S. A noise is worth diffusion guidance, 2024. URL <https://arxiv.org/abs/2412.03895>.

Bai, S., Cai, Y., Chen, R., Chen, K., Chen, X., Cheng, Z., Deng, L., Ding, W., Gao, C., Ge, C., Ge, W., Guo, Z., Huang, Q., Huang, J., Huang, F., Hui, B., Jiang, S., Li, Z., Li, M., Li, M., Li, K., Lin, Z., Lin, J., Liu, X., Liu, J., Liu, C., Liu, Y., Liu, D., Liu, S., Lu, D., Luo, R., Lv, C., Men, R., Meng, L., Ren, X., Ren, X., Song, S., Sun, Y., Tang, J., Tu, J., Wan, J., Wang, P., Wang, P., Wang, Q., Wang, Y., Xie, T., Xu, Y., Xu, H., Xu, J., Yang, Z., Yang, M., Yang, J., Yang, A., Yu, B., Zhang, F., Zhang, H., Zhang, X., Zheng, B., Zhong, H., Zhou, J., Zhou, F., Zhou, J., Zhu, Y., and Zhu, K. Qwen3-vl technical report. *arXiv preprint arXiv:2511.21631*, 2025a.

Bai, S., Chen, K., Liu, X., Wang, J., Ge, W., Song, S., Dang, K., Wang, P., Wang, S., Tang, J., et al. Qwen2. 5-vl technical report. *arXiv preprint arXiv:2502.13923*, 2025b.

Benton, J., De Bortoli, V., Doucet, A., and Deligiannidis, G. Nearly d -linear convergence bounds for diffusion models via stochastic localization. *arXiv preprint arXiv:2308.03686*, 2023a.

Benton, J., Deligiannidis, G., and Doucet, A. Error bounds for flow matching methods. *arXiv preprint arXiv:2305.16860*, 2023b.

Bolya, D., Huang, P.-Y., Sun, P., Cho, J. H., Madotto, A., Wei, C., Ma, T., Zhi, J., Rajasegaran, J., Rasheed, H., et al. Perception encoder: The best visual embeddings are not at the output of the network. *arXiv preprint arXiv:2504.13181*, 2025.

Caron, M., Touvron, H., Misra, I., Jégou, H., Mairal, J., Bojanowski, P., and Joulin, A. Emerging properties in self-supervised vision transformers, 2021. URL <https://arxiv.org/abs/2104.14294>.

Chen, C., Guo, P., Song, L., Lu, J., Qian, R., Wang, X., Fu, T.-J., Liu, W., Yang, Y., and Schwing, A. Carflow: Condition-aware reparameterization aligns source and target for better flow matching. *arXiv preprint arXiv:2509.19300*, 2025a.

Chen, J., Xu, Z., Pan, X., Hu, Y., Qin, C., Goldstein, T., Huang, L., Zhou, T., Xie, S., Savarese, S., et al. Blip3-o: A family of fully open unified multimodal models-architecture, training and dataset. *arXiv preprint arXiv:2505.09568*, 2025b.

Cheng, H. K. and Schwing, A. The curse of conditions: Analyzing and improving optimal transport for conditional flow-based generation. *arXiv preprint arXiv:2503.10636*, 2025.

Degeorge, L., Ghosh, A., Dufour, N., Picard, D., and Kalogeiton, V. How far can we go with imagenet for text-to-image generation? *arXiv preprint arXiv:2502.21318*, 2025.

Dhariwal, P. and Nichol, A. Diffusion models beat gans on image synthesis. *Advances in neural information processing systems*, 34:8780–8794, 2021.

Esser, P., Kulal, S., Blattmann, A., Entezari, R., Müller, J., Saini, H., Levi, Y., Lorenz, D., Sauer, A., Boesel, F., et al. Scaling rectified flow transformers for high-resolution image synthesis. In *Forty-first international conference on machine learning*, 2024.

Ghosh, D., Hajishirzi, H., and Schmidt, L. Geneval: An object-focused framework for evaluating text-to-image alignment. *Advances in Neural Information Processing Systems*, 36:52132–52152, 2023.

Grill, J.-B., Strub, F., Altché, F., Tallec, C., Richemond, P. H., Buchatskaya, E., Doersch, C., Pires, B. A., Guo, Z. D., Azar, M. G., Piot, B., Kavukcuoglu, K., Munos, R., and Valko, M. Bootstrap your own latent: A new approach to self-supervised learning, 2020. URL <https://arxiv.org/abs/2006.07733>.

He, J., Yu, Q., Liu, Q., and Chen, L.-C. Flowtok: Flowing seamlessly across text and image tokens. *arXiv preprint arXiv:2503.10772*, 2025.

Hessel, J., Holtzman, A., Forbes, M., Le Bras, R., and Choi, Y. Clipscore: A reference-free evaluation metric for image captioning. In *Proceedings of the 2021 conference on empirical methods in natural language processing*, pp. 7514–7528, 2021.

Heusel, M., Ramsauer, H., Unterthiner, T., Nessler, B., and Hochreiter, S. Gans trained by a two time-scale update rule converge to a local nash equilibrium. *Advances in neural information processing systems*, 30, 2017.

Ho, J. and Salimans, T. Classifier-free diffusion guidance. *arXiv preprint arXiv:2207.12598*, 2022.

Ho, J., Jain, A., and Abbeel, P. Denoising diffusion probabilistic models. *Advances in neural information processing systems*, 33:6840–6851, 2020.

Hu, X., Wang, R., Fang, Y., Fu, B., Cheng, P., and Yu, G. Ella: Equip diffusion models with ILM for enhanced semantic alignment. *arXiv preprint arXiv:2403.05135*, 2024.

Huh, M., Cheung, B., Wang, T., and Isola, P. The platonic representation hypothesis. *arXiv preprint arXiv:2405.07987*, 2024.

Issachar, N., Salama, M., Fattal, R., and Benaim, S. Designing a conditional prior distribution for flow-based generative models. *arXiv preprint arXiv:2502.09611*, 2025.

Karras, T., Aittala, M., Kynkänniemi, T., Lehtinen, J., Aila, T., and Laine, S. Guiding a diffusion model with a bad version of itself. *Advances in Neural Information Processing Systems*, 37:52996–53021, 2024.

Kingma, D. P. Adam: A method for stochastic optimization. *arXiv preprint arXiv:1412.6980*, 2014.

Kong, L., Tao, M., Liu, Y., Wang, B., Fu, J., Wang, C.-C., and Liu, H. Alignflow: Improving flow-based generative models with semi-discrete optimal transport, 2025. URL <https://arxiv.org/abs/2510.15038>.

Labs, B. F. Flux. <https://github.com/black-forest-labs/flux>, 2024.

Langley, P. Crafting papers on machine learning. In Langley, P. (ed.), *Proceedings of the 17th International Conference on Machine Learning (ICML 2000)*, pp. 1207–1216, Stanford, CA, 2000. Morgan Kaufmann.

Lee, J., Kim, K., and Lee, J. Is there a better source distribution than gaussian? exploring source distributions for image flow matching. *arXiv preprint arXiv:2512.18184*, 2025.

Li, J., Li, D., Xiong, C., and Hoi, S. Blip: Bootstrapping language-image pre-training for unified vision-language understanding and generation. In *International conference on machine learning*, pp. 12888–12900. PMLR, 2022.

Lipman, Y., Chen, R. T., Ben-Hamu, H., Nickel, M., and Le, M. Flow matching for generative modeling. *arXiv preprint arXiv:2210.02747*, 2022.

Lipman, Y., Havasi, M., Holderrieth, P., Shaul, N., Le, M., Karrer, B., Chen, R. T. Q., Lopez-Paz, D., Ben-Hamu, H., and Gat, I. Flow matching guide and code, 2024. URL <https://arxiv.org/abs/2412.06264>.

Liu, Q., Yin, X., Yuille, A., Brown, A., and Singh, M. Flowing from words to pixels: A noise-free framework for cross-modality evolution. In *Proceedings of the Computer Vision and Pattern Recognition Conference*, pp. 2755–2765, 2025.

Liu, X., Gong, C., and Liu, Q. Flow straight and fast: Learning to generate and transfer data with rectified flow. *arXiv preprint arXiv:2209.03003*, 2022.

Ma, C., Xiao, X., Wang, T., Wang, X., and Shen, Y. Learning straight flows: Variational flow matching for efficient generation, 2025. URL <https://arxiv.org/abs/2511.17583>.

Quab, M., Darce, T., Moutakanni, T., Vo, H., Szafraniec, M., Khalidov, V., Fernandez, P., Haziza, D., Massa, F., El-Nouby, A., et al. Dinov2: Learning robust visual features without supervision. *arXiv preprint arXiv:2304.07193*, 2023.

Peebles, W. and Xie, S. Scalable diffusion models with transformers. In *Proceedings of the IEEE/CVF international conference on computer vision*, pp. 4195–4205, 2023.

Pooladian, A.-A., Ben-Hamu, H., Domingo-Enrich, C., Amos, B., Lipman, Y., and Chen, R. T. Q. Multisample flow matching: Straightening flows with minibatch couplings. In Krause, A., Brunskill, E., Cho, K., Engelhardt, B., Sabato, S., and Scarlett, J. (eds.), *Proceedings of the 40th International Conference on Machine Learning*, volume 202 of *Proceedings of Machine Learning Research*, pp. 28100–28127. PMLR, 23–29 Jul 2023. URL <https://proceedings.mlr.press/v202/pooladian23a.html>.

Qin, Q., Zhuo, L., Xin, Y., Du, R., Li, Z., Fu, B., Lu, Y., Yuan, J., Li, X., Liu, D., et al. Lumina-image 2.0: A unified and efficient image generative framework. *arXiv preprint arXiv:2503.21758*, 2025.

Radford, A., Kim, J. W., Hallacy, C., Ramesh, A., Goh, G., Agarwal, S., Sastry, G., Askell, A., Mishkin, P., Clark, J., et al. Learning transferable visual models from natural language supervision. In *International conference on machine learning*, pp. 8748–8763. PMLR, 2021.

Russakovsky, O., Deng, J., Su, H., Krause, J., Satheesh, S., Ma, S., Huang, Z., Karpathy, A., Khosla, A., Bernstein, M., et al. Imagenet large scale visual recognition challenge. *International journal of computer vision*, 115(3): 211–252, 2015.

Salimans, T., Goodfellow, I., Zaremba, W., Cheung, V., Radford, A., and Chen, X. Improved techniques for training gans. *Advances in neural information processing systems*, 29, 2016.

Shi, Y., Bortoli, V. D., Campbell, A., and Doucet, A. Diffusion schrödinger bridge matching. In *Thirty-seventh Conference on Neural Information Processing Systems*, 2023. URL <https://openreview.net/forum?id=qy07OHsJT5>.

Song, J., Meng, C., and Ermon, S. Denoising diffusion implicit models. *arXiv preprint arXiv:2010.02502*, 2020a.

Song, Y. and Ermon, S. Generative modeling by estimating gradients of the data distribution. *Advances in neural information processing systems*, 32, 2019.

Song, Y., Sohl-Dickstein, J., Kingma, D. P., Kumar, A., Ermon, S., and Poole, B. Score-based generative modeling through stochastic differential equations. *arXiv preprint arXiv:2011.13456*, 2020b.

Tong, A., Fatras, K., Malkin, N., Huguet, G., Zhang, Y., Rector-Brooks, J., Wolf, G., and Bengio, Y. Improving and generalizing flow-based generative models with mini-batch optimal transport. *arXiv preprint arXiv:2302.00482*, 2023a.

Tong, A., Malkin, N., FATRAS, K., Atanackovic, L., Zhang, Y., Huguet, G., Wolf, G., and Bengio, Y. Simulation-free schrödinger bridges via score and flow matching. In *ICML Workshop on New Frontiers in Learning, Control, and Dynamical Systems*, 2023b. URL <https://openreview.net/forum?id=adkj23mvB0>.

Tong, S., Zheng, B., Wang, Z., Tang, B., Ma, N., Brown, E., Yang, J., Fergus, R., LeCun, Y., and Xie, S. Scaling text-to-image diffusion transformers with representation autoencoders. *arXiv preprint arXiv:2601.16208*, 2026.

Tschannen, M., Gritsenko, A., Wang, X., Naeem, M. F., Alabdulmohsin, I., Parthasarathy, N., Evans, T., Beyer, L., Xia, Y., Mustafa, B., et al. Siglip 2: Multilingual vision-language encoders with improved semantic understanding, localization, and dense features. *arXiv preprint arXiv:2502.14786*, 2025.

Wang, S., Tian, Z., Huang, W., and Wang, L. Ddt: Decoupled diffusion transformer. *arXiv preprint arXiv:2504.05741*, 2025a.

Wang, X., Cheng, X., Wang, Y., Song, R., and Wang, Y. Vaflow: Video-to-audio generation with cross-modality flow matching. In *Proceedings of the IEEE/CVF International Conference on Computer Vision (ICCV)*, pp. 11777–11786, October 2025b.

Wybitul, E., Rando, J., Tramèr, F., and Fort, S. Representations of text and images align from layer one. *arXiv preprint arXiv:2601.08017*, 2026.

Xie, E., Chen, J., Chen, J., Cai, H., Tang, H., Lin, Y., Zhang, Z., Li, M., Zhu, L., Lu, Y., et al. Sana: Efficient high-resolution image synthesis with linear diffusion transformers. *arXiv preprint arXiv:2410.10629*, 2024.

Xu, S., Ma, Z., Chai, W., Chen, X., Jin, W., Chai, J., Xie, S., and Yu, S. X. Next-embedding prediction makes strong vision learners, 2025. URL <https://arxiv.org/abs/2512.16922>.

Yang, A., Li, A., Yang, B., Zhang, B., Hui, B., Zheng, B., Yu, B., Gao, C., Huang, C., Lv, C., et al. Qwen3 technical report. *arXiv preprint arXiv:2505.09388*, 2025.

Yao, J., Yang, B., and Wang, X. Reconstruction vs. generation: Taming optimization dilemma in latent diffusion models. In *Proceedings of the Computer Vision and Pattern Recognition Conference*, pp. 15703–15712, 2025.

Zheng, B., Ma, N., Tong, S., and Xie, S. Diffusion transformers with representation autoencoders. *arXiv preprint arXiv:2510.11690*, 2025.

Zhou, L., Lou, A., Khanna, S., and Ermon, S. Denoising diffusion bridge models. *arXiv preprint arXiv:2309.16948*, 2023.

Appendix

A. Toy Experiments

A.1. Toy experiments setup

We conduct toy experiments (Fig. 2) on two standard two-dimensional synthetic datasets, Eight with polar angle condition and Two Moons with x -coordinate condition, using the official C^2OT implementation (Cheng & Schwing, 2025). For the conditional flow model, the condition, time and the coordinate x_t are projected into a shared hidden dimension, summed and passed through a 64-dimensional, 10-layer MLP with GELU activations. For the source generator, we use 3-layer MLP, also with GELU activations. We train the network for 20K optimization steps with a batch size of 256, using Adam (Kingma, 2014) with a learning rate of 3×10^{-4} . For visualization in Fig. 2, we generate samples using an Euler sampler with 16 integration steps.

A.2. Condition-dependent Source with Unconditional Flow Model

We conduct additional toy experiments using an *unconditional* flow model to investigate how the learnable condition-dependent source distribution is influenced by conditioning injected into the flow model. Specifically, we compare a conditional source trained with an unconditional flow model $v_\theta(X_t, t)$ against one trained with a conditional flow model $v_\theta(X_t, t, C)$. Note that alignment loss in Sec. 3.2 is not applied for toy experiments.

As shown in Fig. 8 (B), when the flow model does not receive the condition C , the learned source distribution becomes noticeably more discriminative across conditions. This is mainly because in this setting, the source generator must encode condition-specific structure in order to reduce the flow matching loss, resulting in a more informative and well-separated conditional source. However, with unconditional flow model, the vector field is shared across conditions, making it harder for transport trajectories to branch at similar spatial locations.

In contrast, when condition is injected directly into the flow model (i.e., $v_\theta(X_t, t, C)$), the gradient signal received by the source parameters ϕ through the interpolation $X_t = (1 - t)g_\phi(C) + tX_1$ is substantially reduced. Since the flow model can account for most of the conditional information via C , minimizing the flow matching objective places weaker constraints on the source distribution. We further illustrate this in a practical setting in Appx. B.

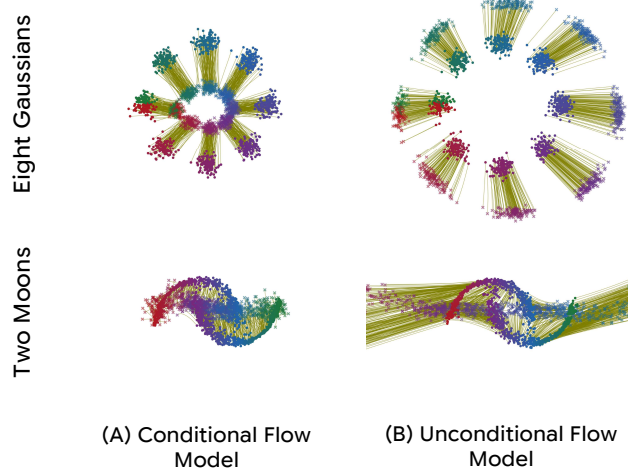


Figure 8. Learned conditional source distributions with conditional vs. unconditional flow models.

A.3. Ill-Conditioned Cases

We further investigate ill-conditioned scenarios in Fig. 9, where the conditioning signal does not sufficiently concentrate the target distribution. Specifically, we consider two extreme cases in which the condition is defined by the ℓ_2 norm of the modes or by the x -coordinate in the Eight Gaussians setting. In these cases, a single condition value can correspond to multiple spatial locations, making the placement of a suitable source inherently ambiguous. Consequently, the learned

source gravitates toward an averaged location—for instance, the midpoint between modes under the x -coordinate condition, or the center of the distribution in the extreme ℓ_2 -norm case—resulting in a more Gaussian-like source.

Despite still encouraging straighter transport paths compared to a fixed Gaussian prior, the learned source distribution in this setting becomes less discriminative across conditions, effectively reverting toward a Gaussian-like baseline (Fig. 9 (A)). This observation aligns with the representation analysis in Sec. 4.3: learnable, condition-dependent source distributions are most effective when the target representation provides sufficient structure to reduce multimodality with respect to the condition.

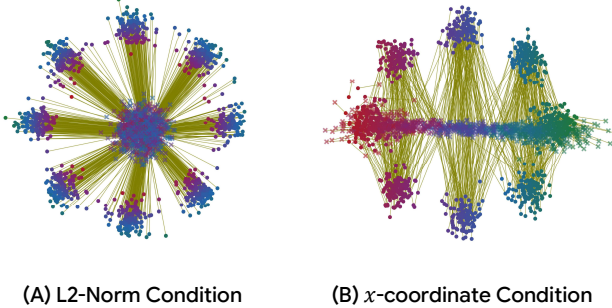


Figure 9. Learned conditional source distributions under ill-conditioned settings.

A.4. Variance Explosion Cases: Stopping Gradient on Target Velocity

In the context of self-supervised learning (Grill et al., 2020; Caron et al., 2021; Xu et al., 2025), stopping gradients is a commonly adopted strategy to prevent representational collapse. Motivated by this practice, one may consider stopping the gradient on the target velocity in Eq. 7 when jointly learning the flow model and the source generator. Concretely, this corresponds to treating the target velocity $\Delta = \text{sg}(X_1 - g_\phi(C))$ as a constant with respect to the source parameters, where sg denotes the stop-gradient operation.

However, as shown in Fig. 10, we find that stopping gradients can cause the explosion of the variance of the learnable source distribution in some cases. This behavior corresponds to a degenerate solution in which the source generator trivially reduces the path variance by allowing the source samples to diverge.

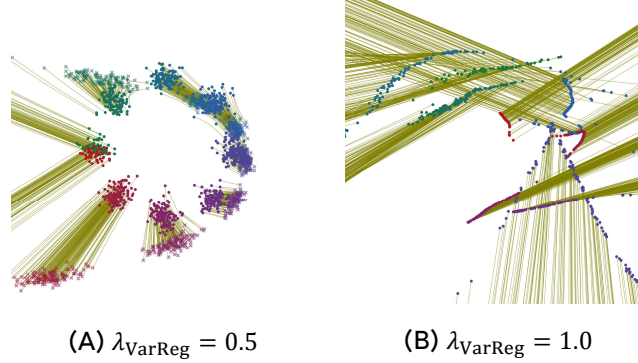


Figure 10. Variance Explosion Case. The variance of the learned source distribution diverges under an unconditional flow model for (B) $\lambda_{\text{VarReg}} = 1.0$.

B. Direct Source-Target Alignment for Complex Training Dynamics

As discussed in Sec. 3.2, conditioning the flow model $v_\theta(\cdot)$ with condition C (i.e., $v_\theta(X_t, t, C)$) can make source learning more challenging from an optimization perspective in complex text-to-image settings. As observed in Appx. A.2, we attribute this to the fact that the source model has less incentive to remain discriminative when conditional information is directly handled by the flow model.

This effect also manifests in practical settings. We evaluate this behavior using LightningDiT with a learnable source generator and the variance regularization term $\mathcal{L}_{\text{VarReg}}$. As shown in Tab. 5, adding conditioning to flow model $v_\theta(\cdot)$ degrades FID relative to the unconditioned counterpart, despite improving CLIP score due to stronger conditional modeling. Consistently, Fig. 11 illustrates that conditioning $v_\theta(\cdot)$ causes the learned source distribution to become less discriminative, indicating that the source struggles to learn meaningful structure.

In contrast, when combined with the alignment loss, we observe improvements in both FID and CLIP score, along with a more discriminative and structured source distribution.

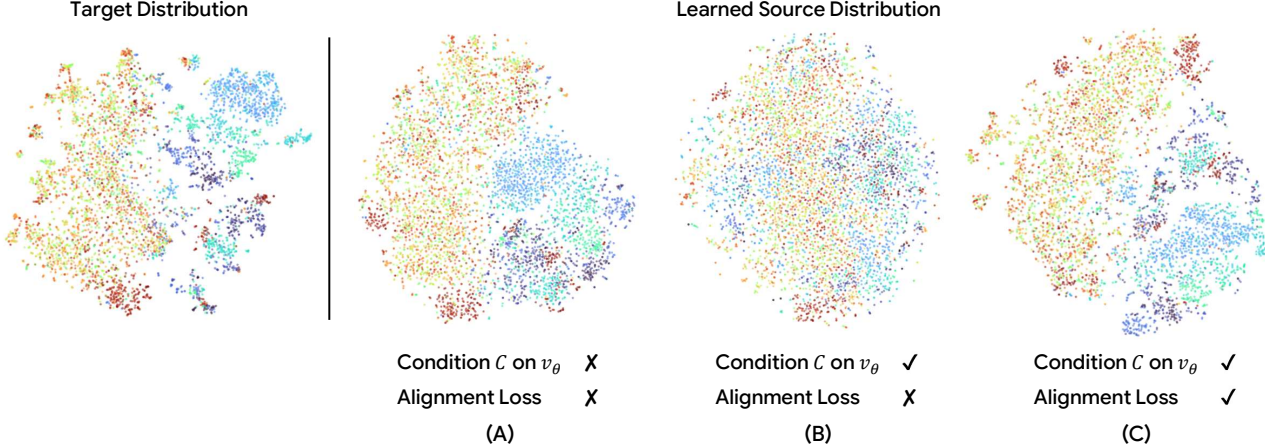


Figure 11. t-SNE visualization of learned source distribution comparing the effects of condition injection and alignment loss.

Table 5. Ablation results analyzing the effects of alignment loss and backbone conditioning.

Flow backbone	Condition C on v_θ	Alignment Loss $\mathcal{L}_{\text{align}}$	FID	CLIP
LightningDiT	\times	\times	3.167	0.3335
	\checkmark	\times	3.188	0.3354
	\checkmark	\checkmark	3.041	0.3363

C. Decomposition of the Flow Matching Objective

We derive the decomposition of the Flow Matching (FM) objective in Eq. (4) into an approximation error term and an intrinsic variance term. Recall that the FM loss is defined as:

$$\mathcal{L}_{\text{FM}}(\theta) = \mathbb{E}_{t \sim p(t), (X_0, X_1) \sim \pi} [\|v_\theta(X_t, t) - \Delta\|^2], \quad (12)$$

where $\Delta = X_1 - X_0$ and $X_t = (1-t)X_0 + tX_1$. Let

$$u_t(x) := \mathbb{E}[\Delta \mid X_t = x] \quad (13)$$

denote the marginal velocity field induced by the coupling π . We rewrite the squared error as:

$$\|v_\theta(X_t, t) - \Delta\|^2 = \|v_\theta(X_t, t) - u_t(X_t) + u_t(X_t) - \Delta\|^2. \quad (14)$$

Expanding the norm yields:

$$\begin{aligned} \|v_\theta(X_t, t) - \Delta\|^2 &= \|v_\theta(X_t, t) - u_t(X_t)\|^2 + \|u_t(X_t) - \Delta\|^2 \\ &\quad + 2\langle v_\theta(X_t, t) - u_t(X_t), u_t(X_t) - \Delta \rangle. \end{aligned} \quad (15)$$

Taking expectation with respect to t and $(X_0, X_1) \sim \pi$, the cross term vanishes:

$$\begin{aligned} \mathbb{E}[\langle v_\theta(X_t, t) - u_t(X_t), u_t(X_t) - \Delta \rangle] \\ = \mathbb{E}[\mathbb{E}[\langle v_\theta(X_t, t) - u_t(X_t), u_t(X_t) - \Delta \rangle | X_t]] \\ = \mathbb{E}[\langle v_\theta(X_t, t) - u_t(X_t), \mathbb{E}[u_t(X_t) - \Delta | X_t] \rangle] = 0, \end{aligned} \quad (16)$$

since $\mathbb{E}[\Delta | X_t] = u_t(X_t)$ by definition. The remaining second term satisfies

$$\mathbb{E}[\|u_t(X_t) - \Delta\|^2] = \mathbb{E}[\text{Var}(\Delta | X_t)], \quad (17)$$

which follows directly from the definition of conditional variance. Combining the above results, the FM objective decomposes as:

$$\mathcal{L}_{\text{FM}}(\theta) = \mathbb{E}_{t, \pi}[\|v_\theta(X_t, t) - u_t(X_t)\|^2] + \mathbb{E}_{t, \pi}[\text{Var}(\Delta | X_t)]. \quad (18)$$

The first term corresponds to the approximation error incurred by learning the marginal velocity field u_t , while the second term is an intrinsic variance determined solely by the coupling π , independent of the model parameters θ .

D. Training and Evaluation Details

We detail the architectures of the source generator in Tab. 6. The architectures of the flow matching backbones used in Tab. 1 and Tab. 4 are provided in Tab. 7. For UnifiedNextDiT(1.3B), which is employed in the scaling experiments, we omit the DDT head since its hidden dimensionality is sufficiently large relative to the latent dimension. In the scaling experiments, the model is pretrained for 400K iterations and subsequently finetuned for 15K iterations. Note that due to differences in internal architectural design, models with the same number of layers and hidden dimensionality may still have different total parameter counts.

All models are trained on a TPUs v5p cluster with Torch/XLA. For evaluation, all experiments are conducted on NVIDIA L40S GPUs, and images are generated from validation captions for all reported metrics. FID, Inception Score (IS), sFID, and Precision–Recall metrics are computed using ADM precomputed statistics (Dhariwal & Nichol, 2021). CLIP Score (Hessel et al., 2021) is computed using the ViT-B/32 model. To balance the scale of source-related objectives with the flow matching loss, we set $\lambda_{\text{VarReg}} = 5.0$ and $\lambda_{\text{align}} = 1.0$ across all experiments.

For the source generator, we take the input text embedding $\mathbf{e}^{\text{text}} \in \mathbb{R}^{N \times d}$, where N denotes the text sequence length and d is the text embedding dimension. We adopt a Perceiver-style architecture (Li et al., 2022) with S learnable query tokens, where S matches the flattened image-token sequence length. The image embedding $\mathbf{e}^{\text{img}} \in \mathbb{R}^{S \times D}$ serves as the target representation, where D is the image embedding dimension. Since flow matching requires the source and target to lie in the same space, we use cross-attention to map the query tokens conditioned on \mathbf{e}^{text} into the image embedding space $\mathbb{R}^{S \times D}$. For architectures such as LightningDiT (Yao et al., 2025) and MMDiT (Esser et al., 2024) that require AdaLN-based modulation, we use the pooled text representation when available; otherwise, we fall back to a mean-pooled text embedding.

Table 6. Architectural details of the source generator used in our experiments.

Source Generator		
Architecture		
Input dim.	768	1024
Hidden dim.	768	768
Num. layers	8	8
Num. heads	12	12
Params	77M	78M
Text-encoder	CLIP	Qwen-3
Max length	77	128

Table 7. Architectural and optimization details of flow matching backbones used in our experiments.

	LightningDiT	MMDiT	UnifiedNextDiT	UnifiedNextDiT [†]	UnifiedNextDiT(1.3B)
Architecture					
Downsample Ratio	16 × 16	16 × 16	16 × 16	16 × 16	14 × 14
Latent dim.	768	768	768	768	1152
Num. layers	12	12	14	16	20
Hidden dim.	768	768	864	864	1728
Num. heads	12	12	12	12	16
DDT Head					
Num. layers	2	2	2	2	
Hidden dim.	2048	2048	2048	2048	✗
Num. heads	16	16	16	16	
Params	294M	418M	414M	471M	1.24B
Base-encoder	DINOv2	DINOv2	DINOv2	DINOv2	SigLIP2
Optimization					
Batch Size	1024	1024	1024	1024	256
Optimizer	AdamW	AdamW	AdamW	AdamW	AdamW
base lr	2×10^{-4}	2×10^{-4}	2×10^{-4}	2×10^{-4}	2×10^{-4}
(β_1, β_2)	(0.9, 0.95)	(0.9, 0.95)	(0.9, 0.95)	(0.9, 0.95)	(0.9, 0.95)

E. Imagenet Captioned Dataset

As modern text-to-image frameworks increasingly emphasize scaling, there is no well-established setting for component-wise analysis (Degeorge et al., 2025). To enable controlled component-wise experiments at a manageable scale, we construct a captioned dataset based on ImageNet-1K (Russakovsky et al., 2015). Detailed image captions are generated using Qwen3-VL-8B-Instruct (Bai et al., 2025a). Examples from the resulting dataset are shown in Fig. 12.



A blue and orange leather cuirass with circular cutouts and silver rivets, featuring shoulder pauldrons with decorative cutouts, resting on grass and rocks.



A young man with blonde hair and glasses, wearing a white button-up shirt and a white blazer, holds a cello with his left hand on the neck and his right hand holding the bow, looking ...



A blue-and-yellow macaw perched on a weathered tree branch, its vibrant blue wings and tail feathers contrasting with its bright yellow chest and underbelly, sharp black beak ...

Figure 12. Examples of detailed image–caption pairs from the constructed captioned ImageNet-1K dataset.

F. Gradient Variance

We report the variance of gradients of the flow model $v_\theta(\cdot)$ induced by the Flow Matching loss, i.e., $\text{Var}(\nabla_\theta \mathcal{L}_{\text{FM}})$, across the interpolation time t (Fig. 3). To compute gradients, we select five attention layers uniformly sampled from the flow backbone and measure the gradients of the MLP parameters that project inputs to the query, key, and value vectors. The reported variance is further averaged across the selected layers. Due to the small magnitude of individual gradient components, we compute the variance element-wise and report the sum across dimensions. Experiments are conducted using 20K samples from the ImageNet-1K (Russakovsky et al., 2015) training set and a model trained for 100K steps. We use `torch.func.vmap` to efficiently compute per-sample gradients.

G. Detailed Related Works

Flow Matching. Flow Matching (FM) learns an unbiased velocity field that defines a continuous probability path between a source distribution and a target distribution (Lipman et al., 2022; Liu et al., 2022; Lipman et al., 2024). Owing to its conceptual simplicity and strong generative performance, FM has emerged as a popular framework for denoising-based generative modeling. In contrast to conventional diffusion formulation (Ho et al., 2020), FM does not restrict the prior distribution to a standard Gaussian (Liu et al., 2025). Despite this flexibility, the choice of source distribution and the possibility of learning it remain largely underexplored.

Optimal Transport Coupling. During training flow matching, independent coupling between a Gaussian source distribution and the target distribution induces suboptimal training trajectories with intersections, resulting in non-straight flows and high-variance gradients in the FM losses. To mitigate this issue, Tong et al. (2023a); Pooladian et al. (2023); Kong et al. (2025) propose coupling source and target samples using minibatch-level optimal transport plans. Cheng & Schwing (2025) analyze OT coupling in conditional generation settings. They show that such coupling strategies can induce conditionally skewed source distributions, which hampers effective flow learning, and therefore propose a condition-aware OT coupling method. Despite these advances, existing OT-based coupling methods typically involve inefficient optimization procedures and remain ineffective for complex, high-dimensional generation tasks (Cheng & Schwing, 2025). On the other hand, our method learns condition-dependent source–target couplings in an end-to-end manner, which effectively improves flow matching for continuous conditional generation.

Condition-dependent Source Distributions. Several recent works investigate the design of condition-dependent source distributions for conditional flow matching. Issachar et al. (2025) propose to pretrain a condition-dependent source using a mean squared error objective to match source–target pairs prior to flow model training. Ahn et al. (2024) train a source generator to reproduce noise obtained from diffusion inversion, leveraging a pretrained diffusion model. Recent analysis-driven work further studies source distribution design from an optimization and geometric perspective, deriving practical guidelines through interpretable simulations (Lee et al., 2025). More recently, Chen et al. (2025a) introduce CAR-Flow, providing theoretical insights that simple conditional shifting operations can prevent collapse in reparameterized distributions. While these approaches demonstrate that incorporating conditioning information into the source is feasible, they often rely on multi-stage training or have not been extensively validated on large-scale and highly complex conditional generation tasks such as text-to-image synthesis.

Flow Matching Between Distributions. Another line of work studies flow matching between different distributions or modalities. Early bridging models (Shi et al., 2023; Tong et al., 2023b; Zhou et al., 2023) mainly focus on closely related domains (e.g., image-to-image). CrossFlow (Liu et al., 2025) and VAFlow (Wang et al., 2025b) extend flow matching to cross-modal settings, such as text-to-image or video-to-audio, often using variational encoders or contrastive objectives. FlowTok (He et al., 2025) further explores learned token-level source representations. These methods primarily aim to enable distribution-to-distribution transport, and typically report modest improvements in generative quality compared to standard conditional flow matching. Our work differs in focus: rather than designing new transport objectives, we study how learning an appropriate, condition-dependent source distribution fundamentally alters flow matching dynamics, leading to improved optimization and generative performance in complex conditional settings.

H. Additional Quantitative Results

Tab. 8 reports the full benchmark comparison on GenEval (Ghosh et al., 2023), and Tab. 9 reports the full benchmark comparison on DPG-Bench (Hu et al., 2024) between standard FM and CSFM.

Table 8. Category-wise performance comparison of standard FM and CSFM on GenEval.

Model	Single Obj.	Two Obj.	Counting	Colors	Position	Color Attri.	Overall↑
Standard FM	0.99	0.87	0.63	0.85	0.76	0.53	0.77
CSFM (Ours)	0.98	0.88	0.65	0.90	0.79	0.59	0.80

Table 9. Category-wise performance comparison of standard FM and CSFM on DPG-Bench.

Model	Global	Entity	Attribute	Relation	Other	Overall↑
Standard FM	81.46	87.04	85.06	92.80	75.60	78.31
CSFM (Ours)	84.80	88.80	85.93	93.23	76.00	81.11

I. Additional Qualitative Results

We present qualitative results comparing fixed and learnable source distributions. Fig. 13 and Fig. 14 present qualitative comparisons using the model trained for 100K steps in Sec. 4.1, evaluated on ImageNet-1K (Russakovsky et al., 2015) validation set, with a 50-step Euler ODE sampler. Fig. 15 further demonstrates model performance on text involving **complex relationships** and **multiple objects**, using the same 50-step Euler ODE sampler. Fig. 16 and Fig. 17 present qualitative comparisons using the scaled UnifiedNextDiT (1.3B). While standard T2I benchmarks show limited gains due to score saturation, the learnable-source model consistently yields samples with **stronger visual quality and perceptual coherence**.

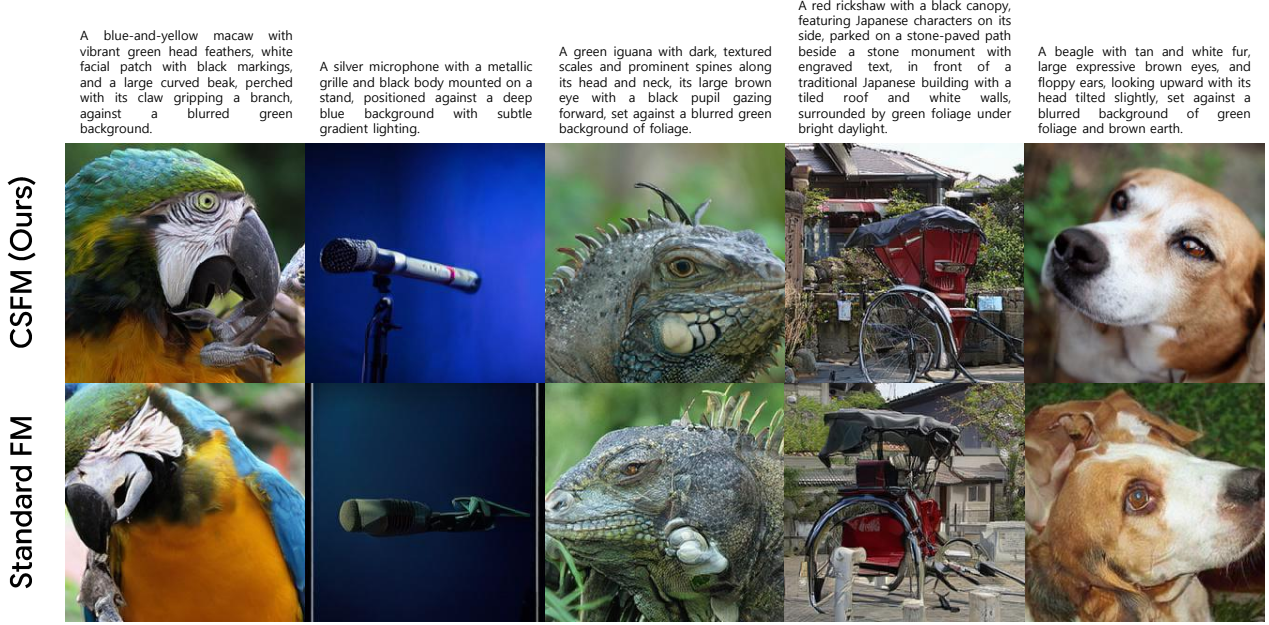


Figure 13. Qualitative comparison between fixed and learned source distributions on ImageNet-1K (Russakovsky et al., 2015).



Figure 14. Qualitative comparison between fixed and learned source distributions on ImageNet-1K (Russakovsky et al., 2015).

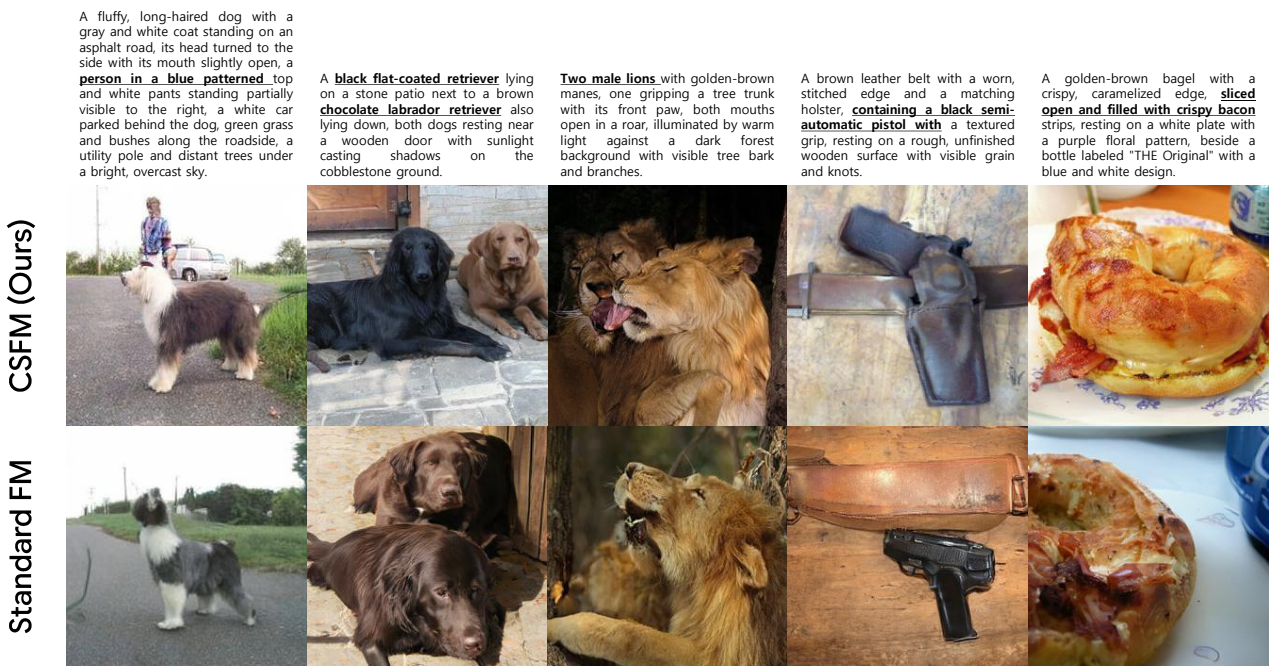


Figure 15. Qualitative comparison between fixed and learned source distributions for prompts with multiple objects and complex relationships, on ImageNet-1K (Russakovsky et al., 2015).

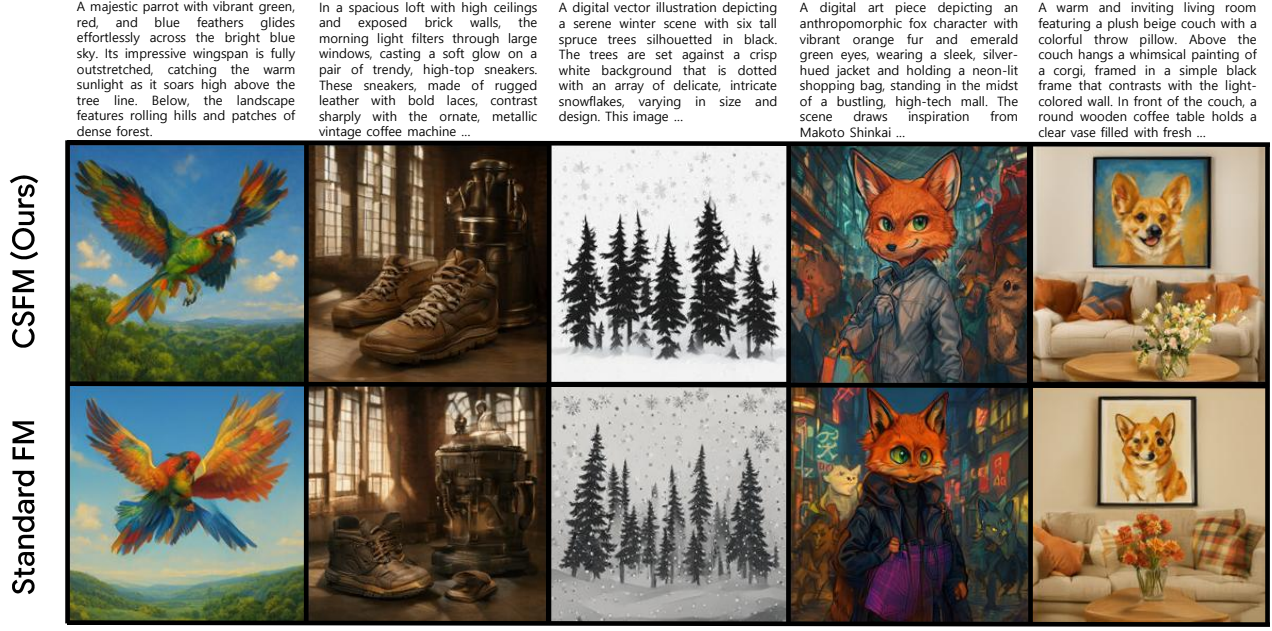


Figure 16. Qualitative comparison between fixed and learned source distributions using UnifiedNextDiT (1.3B).



Figure 17. Qualitative comparison between fixed and learned source distributions using UnifiedNextDiT (1.3B).